Hindawi
Advances in Civil Engineering
Volume 2024, Article ID 8836116, 14 pages
https://doi.org/10.1155/2024/8836116

Research Article

Comparative Study on the Reinforced Sand-Bed and the Stone Column in Improving the Clay Deposit Supporting Isolated Footing

Premalatha Krishnamurthy and Priyadharshini Maniam Rajan

Division of Soil Mechanics and Foundation Engineering, Department of Civil Engineering, College of Engineering Guindy, Anna University, Chennai 600025, Tamil Nadu, India

Correspondence should be addressed to Priyadharshini Maniam Rajan; priyadharshini.civil@gmail.com

Received 18 October 2023; Revised 22 December 2023; Accepted 18 January 2024; Published 31 January 2024

Academic Editor: Cun Hui

The working mechanism of a geotechnical structure can be understood from the deformations and the vertical stresses in the soil media. This article attempts to study the deformation, vertical stress development, and distribution of improved clay deposits carrying a single isolated footing. Through PLAXIS 3D software, numerical analyses were conducted for the ground improvement methods, such as the geogrid reinforced sand-bed (GRSB) and ordinary and geogrid encased stone column installation (OSC and GESC). In GRSB, the results show that the stresses were maximum at the sand–clay interface at a depth of 0.67 B (B—footing width). It is proposed to place an additional layer of geogrid at the interface, and it must be within the critical depth, i.e., the width of the footing. Furthermore, for the current study, the stiffness of the geogrid in the sand layer greater than 500 kN/m was insignificant in soil improvement, whereas the optimum axial stiffness of the stone column encasement was 1,000 kN/m based on the stress concentration factor. The stone column installation improved the clay layer even below the depth of 0.67 B, improving the capacity of clay to carry higher vertical stresses on par with the stone columns. The GRSB carried higher vertical stresses than the unimproved ground. However, the OSC and GESC could carry vertical stresses higher than the GRSB. This knowledge can allow the practitioners to decide the depth of placement of the reinforcement and also to choose an alternate if one method is not feasible for the site.

1. Introduction

Improving the weak soil deposits is the most necessary in the present-day scenario due to the lack of suitable areas for construction. Ground-improvement techniques strengthen weak soil deposits with different working mechanisms. The techniques, such as placement of reinforced sand-bed and installation of stone columns, are given due importance in this paper. Several studies are related to these two techniques. In most of them, the geosynthetics applications focussed on bearing capacity improvement [1–3] and settlement reduction [3, 4].

The study of vertical stress development and its distribution in the geogrid-reinforced sand-bed (GRSB) layer below the footing was insignificant in previous research. The initial study on vertical stress distribution theory proposed by Boussinesq [5] is still widely used to analyse the stresses and displacements in a homogeneous, isotropic, elastic, semi-infinite medium when subjected to a vertical point load. Soil reinforcement using geosynthetics leads to a variation in the vertical stress development and distribution, which has not been widely researched. Recently, studies have attempted to explore such changes in the vertical stress influenced by geosynthetic reinforcement within homogeneous [6] and layered soil systems [7], which ultimately explains the settlement reduction.

El Sawwaf [8] reported from numerical studies that reinforcing the sandy layer with geogrid improved the footing performance and reduced the settlement compared to the unreinforced sand layer. A similar study portraying the beneficial effects of geogrid reinforcement by Yadu and Tripathi [9]

reported the best adoptable geogrid length as four times the width of the strip footing. Demir et al. [10], in continuation with the large-scale field tests [11], also conducted numerical investigations exploring the influence of the thickness of the granular fill, the number of geogrid reinforcements, and the depth of the reinforcement. Subinay and Deb [12] conducted model tests on footings with different aspect ratios and reported that reinforcing the granular bed with two geogrid layers would be more beneficial. The depth of the first reinforcement was 0.25 and 0.375 times the footing width for the square and rectangular footing, respectively.

The axial stiffness of the reinforcement is an essential parameter in studying the functioning of geosynthetic reinforcement. Deb et al. [13] numerically studied the multilayered reinforced granular bed. It was reported that the increase in reinforcement layers influenced the stress distribution in the soil. Also, the settlement of the soil is reduced considerably when the axial stiffness of the reinforcement is between 4,000 and 5,000 kN/m. A contrary finding by Latha and Somwanshi [14] reported that the reinforcement's tensile strength did not significantly improve the strength of the reinforced soil compared to the reinforcement's layout and configuration. Niculescu-Enache [15], from detailed numerical analyses, noted that the inclusion of geosynthetic reinforcement resulted in stress concentration in a smaller area below the footing. The author reported that the reinforcement inclusion led to a smaller pressure bulb than the unreinforced soil, contrary to the results reported in the present study. A new study on bearing capacity improvement by the wrap-around reinforcement technique and its use in limited land areas was also reported [16–22]. Jaiswal et al. [21] conducted a detailed parametric study in which the influence of the reinforcement width and the geogrid axial stiffness effect on the ultimate load-carrying capacity and the settlement have been determined. The results showed that the optimum reinforcement width is 1.5 times the footing width, and the optimum geogrid axial stiffness is 1,000 kN/m. The author also emphasised the significance of the interface effect between the soil and the geogrid layer in the design purpose. Dasaka et al. [22] studied the wrap-around reinforcement technique by numerical and regression analyses. In this paper, the authors developed equations to determine the ultimate load-bearing capacity of the reinforced soil deposit for axial stiffness of geogrid up to 2,000 kN/m for a specific field condition.

The performance of the geogrid-encased stone columns (GESC) and ordinary stone columns (OSC) was studied based on the settlement reduction and the stress concentration factor (SCF) [23]. The stresses developed in the stone columns, and clay are expressed using the SCF, which indicates the intensity of the vertical stress transferred from the footing to the stone column and the surrounding soil. Fattah and Majeed [24] studied the effect of different parameters like length-to-diameter ratio (L/d), area replacement ratio, and thickness of the stone cap (granular layer) on the settlement reduction and the bearing capacity improvement of the stone columns. GESC performed better than OSC for all the L/d ratios. Also, Fattah and Majeed [25] performed similar analyses on stone columns to study the effect of the parameters mentioned above on the cohesive strength (c_u) of the soil. The author observed the improvement in bearing capacity when the area replacement ratio (a_r) increased beyond 25% for GESC. Also, the lateral displacement of the GESC decreased to a large extent due to the provision of the encasement material. The maximum L/d ratio for OSC was 7–8 and 10–11 for c_u 20–40 and 10 kPa, respectively. For GESC, the maximum (L/d) was observed as 7–8 for all values of c_u.

A new study on the effect of soil arching in embankments over stone column-reinforced soil was reported by Fattah et al. [26, 27]. It was found that the effect of the soil arching in embankments was a function of the ratio of the embankment height (h) to the clear spacing between the columns (s), i.e., (h/s). The soil arching effect was prominent for the ratio $(h/s) > 2.2$ for both OSC and GESC, and no soil arching occurred for $(h/s) < 1.2$ and 1.4 in OSC and GESC, respectively. The increment of SCF values also indicates the soil arching effect with the increase in the h/s ratio. The study emphasises the significance of soil arching in the working mechanism of stone columns supporting embankments. Similarly, the additional stress the stone column carries due to geogrid encasement also plays an important role. The provision of encasement around the stone columns improves the bearing capacity and reduces the settlement of the composite ground [28].

The literature review shows the improvement in bearing capacity by providing the GRSB or OSC/GESC. However, the development of stresses within the soil medium needs to be assessed to understand the capability of one type of improvement over the other. This study explores the vertical stress development and distribution in the composite clay—GRSB and the stress concentration in the composite clay—OSC and GESC ground by observing the soil media. The mentioned points are discussed in this paper; additionally, the ground improvement method, which performs better based on vertical stress, is also proposed.

2. Validation of the Numerical Modelling

2.1. Numerical Simulation of Improved Clay Deposit. Numerical Modelling was carried out using the PLAXIS 3D finite element software. The model dimensions were chosen based on the field test details. Soil layers were simulated using the "borehole" option on the "soil" tab. The properties of the material were given as input parameters. The material models were selected as Mohr–Coulomb (M–C) for the soil layers, linear elastic for footing, and built-in geogrid model for geogrids. The M–C material model can adequately simulate the behaviour of soil layers in numerical modelling [29–32]. The geogrid is chosen to behave elastically with isotropic behaviour. The input for the Geogrid model is the axial stiffness in the longitudinal direction. The axial stiffness of the geogrid can be obtained as the ratio of the maximum tensile strength of the geogrid to a percentage of strain, which can be determined experimentally. The increase in the stiffness value directly indicates the increase in the geogrid's tensile strength. Therefore, in this study, the geogrid strength is identified by axial stiffness.

The model meshed using the medium-size element distribution after completing the modelling part. Soil layers and stone columns were meshed using 10-noded tetrahedral elements, whereas the footing and the geogrid were meshed using the 6-noded plate and geogrid elements, respectively [33]. So, to model the soil continuum and the geogrid layer separately, the elements were also chosen differently. The interface around the geogrid and the surrounding clay deposit was created and made of 12-noded elements. When the mesh is generated, the node pairs are created between the soil-interface and the interface-geogrid with identical pairs of nodes to form the continuity of the soil-interface-geogrid elements, a built-in process. The interface element strength is reduced manually to about two-thirds of the surrounding soil to accommodate the disturbance caused by installing the stone column with encasement.

In continuation with meshing, the actual working method is simulated from the initial phase in the staged construction. The initial phase consists of the undisturbed soil deposit without any foundation element. The field construction sequence for the GRSB and OSC/GESC and footing were simulated in the subsequent phases for the validation and the present study. The GRSB and OSC/GESC composite foundation system was analysed, and the results are discussed in the following sections.

2.2. Validation-1: GRSB Improved Clay Deposit

2.2.1. Model, Input Parameters, and Numerical Simulation. A large-scale field test data for GRSB improved clay deposit performed by Demir et al. [11] was chosen to validate the modelling scheme. The field test was performed on a test pit area of 2.8 m × 2.8 m with a 2 m depth. With 2 m depth as the existing ground level (GL), the levels of the soil layers present below were fixed. The boundary interferences were avoided by choosing the model dimension as 15 m × 15 m × 16 m. The model dimensions have been extended to a few footing widths to obtain a complete extent of the influence zone. The circular footing of 0.9 m diameter (D), 0.03 m thickness made of mild steel, was modelled using a plate element. A schematic representation of the GRSB-installed clay deposit is shown in Figure 1.

The input properties for the numerical modelling were obtained from the field details and the standard publications. The field test data comprised the SPT-N values and the Menard modulus. The missing soil properties were obtained using the soil correlations from the standard publications [30, 34–40]. The Menard modulus correlation $E_m/E = \alpha$ was used to obtain Young's modulus of the soil. The relationship between the moduli was studied by Fawaz et al. [40] and was reported to be between 0.55 and 1. For the present study, the value of α was taken as 1, and Young's modulus was calculated.

The unit weight and Poisson's ratio of the soil were obtained from the literatures [36, 41] and [37], respectively. The SPT-N value for limestone was correlated with the study of Cole and Stroud [39], and the shear strength values were obtained from it. The nature of limestone in the field was not provided explicitly. However, with the SPT-N values, it can be understood that limestone was not as strong as a rock but may have been in weathered conditions in the form of soil. With that as the assumption, the properties of limestone were taken from the correlations for hard clay [37]. The properties thus obtained are shown in Table 1.

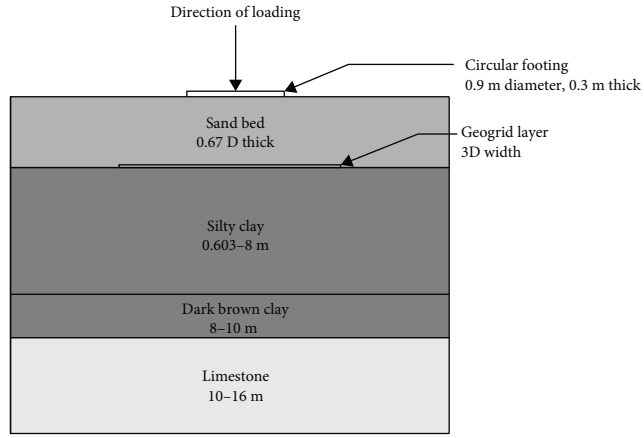

Figure 1: Schematic layout of the GRSB-installed clay deposit.

The geogrid was placed at a depth of 0.67 times the footing diameter in the granular bed, equal to 0.603 m. The geogrid used for the field test had a maximum tensile strength of 60 kN/m. The validation reference paper [11] did not disclose the strain percentage at the maximum tensile strength. So, to determine the geogrid axial stiffness, the strain percentage of the SECUGRID® geogrid data was taken from Demir et al. [11]. The material properties, as provided by the manufacturer, were as follows: For 2% strain and 22 kN/m tensile strength, the geogrid axial stiffness (J) was 1,100 kN/m. Similarly, for 5% strain and 48 kN/m tensile strength, the geogrid axial stiffness (J) was 960 kN/m. From the available two strain values, a strain of 2% with a tensile strength of 22 kN/m [11] was used for the numerical analysis. The justification for selecting the same is given in the following sections.

(1) Guidelines from BS 8006-1:2010: Code of Practice for Strengthened/Reinforced Soils and Other Fills. Based on the guidelines of BS 8006-1:2010, Clause 8.3.2.11 [42], the geogrid provided as the basal reinforcement for the structure constructed upon the weak soil deposit may have an allowable strain reduced to 3% to satisfy strain compatibility. Therefore, the geogrid strain was selected as 2%.

(2) Strain Compatibility. Understanding the strain compatibility is necessary to determine the combination of resistances offered by the material using numerical analysis [43]. A study on strain compatibility was carried out to find the strain at which the geogrid functions. The strain compatibility between the sand and the geogrid was obtained by determining the settlement. A research paper carried out a similar measurement in geogrid-reinforced sand below the centre of the footing and along the geogrid length [6]. From the observations, the authors reported that the strain was high below the centre of the footing and, in addition, highlighted the importance of strain compatibility between the sand deposit and geogrid.

Table 1: Soil properties for the Validation-1.

Soil	Dense sand	Silty clay	Dark brown clay	Limestone
Layer thickness (m)	0–0.603	0.603–8	8–10	10–16
Material model	M–C	M–C	M–C	M–C
Unit weight, γ (kN/m^3)	21.7	18	20	21
Young's modulus, E (kPa)	30,000	3,400	4,250	50,000
Poisson's ratio, υ	0.3	0.4	0.4	0.2
Cohesion, c_u (kPa)	15	75	38	198
Friction angle, φ (°)	43	—	—	—

In the present study, the strain in the soil deposit measured above the geogrid was determined to be 0.46%. So, for compatibility, the geogrid must undergo an equivalent strain. The geogrid strain values of 0.5% and 1% may yield tensile strength of 5.5 and 11 kN/m obtained by extrapolating the given geogrid values [11]. Again, these values may yield an axial stiffness equal to 1,100 kN/m as there is a linear relation; hence, the results would be the same for 0.5%, 1%, and 2% strain. The geogrid must have some strain to mobilise the tensile strength, and as the axial stiffness was similar to that of 2% strain, a minimum value of 2% strain was chosen from the given material property [11] for the analysis.

(3) Linear Behaviour of the Geogrid in the Initial Stage of Loading. When the reinforced soil deposit is loaded, the geogrid reinforcement works efficiently by undergoing tensile strain when aligned in the direction of the tensile strain in the soil. Under loading, the geogrid has to undergo higher strain to mobilise its tensile strength [43]. In the field, the load-settlement behaviour is initially linear, and due to soil nonhomogeneity, the trend may become nonlinear. In numerical modelling, the material model controls the behaviour of the soil and the geogrid elements and exhibits linear behaviour in the initial loading. A nonlinear trend appears once a higher strain is attained; the field and the numerical analysis result would converge at this point of a higher strain. In the present study, such convergence between the field and the numerical result may occur at a higher strain value and loading condition. Generally, the geogrid tested for tensile strength exhibits a linear trend in lower strains (~2% to 3%), and then the nonlinearity appears with an increase in the strain. The trend was mainly observed in the PP type of geogrid [44], which is similar to the SECUGRID® [11]. So, the strain of 2% was selected, with a linear trend in agreement with the published results. With this strain value and axial stiffness of the geogrid, the numerical analysis was carried out for the GRSB over soft clay deposit.

2.3. Validation-1—Discussion. The field test pressure of 440 kN/m^2 was applied on the footing, and the model was analysed. The applied pressure-settlement behaviour of the GRSB improved clay was observed from the output results. The same has been plotted along with the field result. The result of the validation for the applied pressure (q) and settlement/diameter (S/D)% is shown in Figure 2. Only a few points from the cited paper [11] were chosen, reflecting the curve's trend.

From the numerical analysis result and the comparison with the field test value, it was observed that the percentage

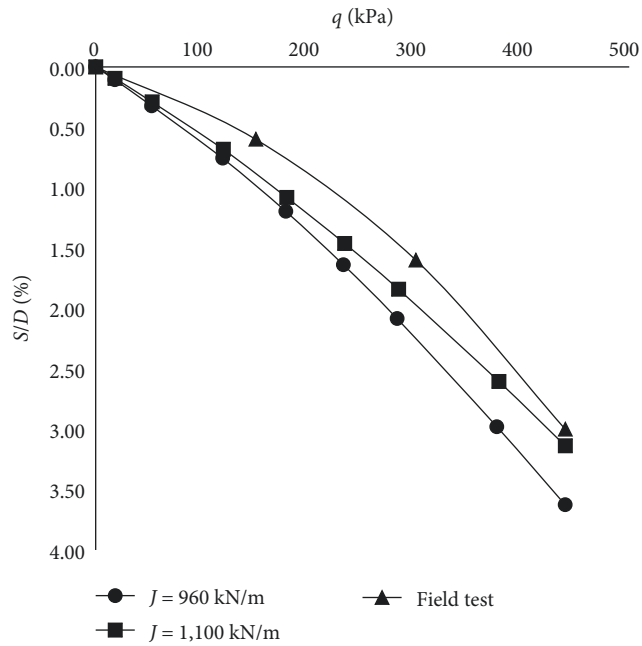

Figure 2: Validation-1—graph comparing field test [11] and PLAXIS 3D results.

difference in the settlement between the field test and the 2% strain assumption case was 5%. In a similar analysis, for the 5% strain and an axial stiffness (J) of 960 kN/m, the settlement value was 32.6 mm. The percentage difference is about 21% compared to the field test value. So, the assumption of 2% strain in the numerical analysis is in closer agreement with the field value. Therefore, the strain compatibility exists between clay and the geogrid for the value of 2%, implying that the modelling is reliable. Also, with the increase in the geogrid axial stiffness (J), the reinforced soil undergoes lesser settlement for an applied pressure, as shown in Figure 2, i.e., an increase in the axial stiffness provides additional strength to the soil. The settlement reduction signifies the numerical model's ability to simulate the geogrid behaviour with the axial stiffness as the reliable input.

Similarly, the reliability of the numerical model can be observed from the following explanations.

2.3.1. Concept of the Equivalent Footing of the GRSB and Comparison of the Numerical Analysis with Boussinesq's Theory. The geogrid layer can transfer the loads with an angle of 45° for the stress distribution. The same was experimentally

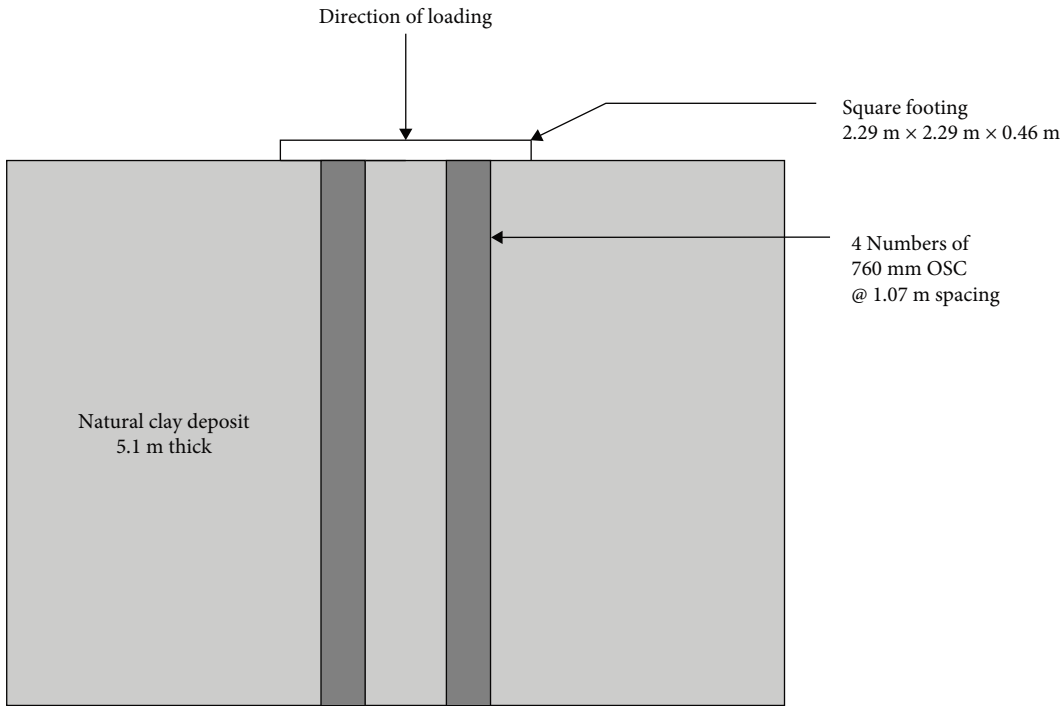

Figure 3: Schematic layout of the stone column-installed clay deposit.

proven in past studies [45, 46]. With a distribution of 45°, the area below the geogrid reinforced foundation can act as the equivalent footing. Due to the geogrid, the equivalent footing distributes the footing pressure to a broader and deeper depth in the soil medium. So, even a higher loading from the footing is distributed in lesser percentages to the weaker deposits, strengthening the overall foundation and reducing the settlement. Meanwhile, the stress distribution in unreinforced weak soil deposits is narrow, leading to failure as the soil cannot bear higher footing pressure.

The same concept was observed when studying the influence zones below the footing. The equivalent footing concept is set below the reinforced foundation, and the influence zone moves deeper than the influence zone in natural clay deposits. The observation was made by comparing the influence zone with Boussinesq's pressure distribution for uniformly loaded circular footing. As per Boussinesq, the isobar of 0.05q was at a depth of 5.3 R_e, equal to 5.6 m, laterally at 2.3 R_e, equal to 2.42 m, where R_e is the equivalent radius of the footing equal to 1.053 m. The R_e was determined from the equivalent width concept. In the present study, the point of negligible settlement beyond the 0.05q isobar was approximately at a depth greater than 5.7 m and laterally at 3.9 m. The variation in the influence zone dimensions may be due to the meshing of the model and iteration processes. Similarly, the vertical stresses and the settlement measured at a depth for footing on natural clay deposit, sand layer, and the geogrid reinforced sand bed showed a decreasing trend exhibiting the lesser stress distribution to deeper depths. The values are comparable; thus, from observation, the model's efficiency in simulating the geogrid reinforced foundation equivalent to the field condition is reliable.

It has to be agreed upon that PLAXIS 3D has its limitations, and possibly, the results obtained would be slightly different from the theoretical and field solutions, which is within an agreeable range, and the nonhomogeneity of soil can lead to some variations in results. The material property and state may also lead to variation in the influence zone below the reinforced foundation. The variation of 5% in the settlement values may be attributed to the material properties, material model, model dimensions, and meshing in the numerical modelling. The numerical material model expressed a slightly linear trend, but the result is comparable. This observation shows that the material models and the meshing scheme can reasonably recreate the field problem numerically.

2.4. Validation-2: Stone Column-Installed Clay Deposit

2.4.1. Model, Input Parameters, and Numerical Simulation. A field test was conducted on a square footing with 2.29 m sides placed on a 4-stone column group arranged in a square with a spacing of 1.07 m [47]. The stone column with a diameter of 0.76 m was installed 5.1 m into the alluvial clay layer. A schematic representation of the stone column-installed clay deposit is shown in Figure 3.

A numerical model was developed using the PLAXIS 3D software simulating the field test. The model dimension of 10 m × 10 m × 14 m was chosen after several trials to avoid any interference from the boundaries on the deformation pattern of OSC/GESC. Similar to the field, the footing was modelled as a plate element with the elastic model. The footing properties and the soil and stone column parameters used for the numerical analysis are listed in Tables 2 and 3 and available in the literature [47], except the footing properties, which were assumed based on the standard values [48].

Table 2: Properties of footing installed in the field for Validation-2 [47, 48].

Shape of the footing	Square
Size of the footing	2.29 m × 2.29 m (0.46 m thick)
Material model type	Elastic
Unit weight, γ (kN/m^3)	25
Young's modulus, E (MPa)	27,000
Poisson's ratio (ν)	0.15

The material model assigned was M–C for both clay deposits and stone columns because of the adequacy of the model in simulating the load-settlement response. The M–C was commonly adopted in the numerical study of stone column problems [25, 29, 32].

2.5. Validation-2—Discussion. The footing was loaded to the maximum field-testing load of 1,700 kN. The field curve from the load–settlement curve was replotted from the literature (Figure 6(b) of [47]) and is shown in Figure 4. The load–settlement curve obtained from the numerical analysis was a good fit with the field result for the end settlement. There was a difference in the settlement in the middle region of the load–settlement curve. The result of the curve's nonlinear portion is conservative, as the settlement was higher for a lesser load than the field measurement. Pham and White [49] performed numerical analysis for this same field condition using an axisymmetric finite element model, and the result is also shown in Figure 4. The model predicted the capacity of the improved foundation to be 880 kN [49] against a field value of 820 kN for a 10 mm settlement, whereas, in the current study, the material model exhibited a capacity of 700 kN for the same settlement. Beyond this point, the predicted results from the literature [49] slightly overestimate the loading for the final settlement, whereas, in the current study, the numerical scheme employed gave almost the same result as that of the field condition.

The variation may be attributed to the material properties, model dimensions, meshing, and the iterations in the calculation part. However, the material model chosen has accurately predicted the final settlement value. Also, as mentioned in the previous validation case, the M–C model reflects the nonlinear behaviour of the soil when a higher loading is reached. The comparison with the same author's field study and the numerical analysis shows that the numerical modelling scheme can simulate the field conditions with appropriate material properties. The limitations of the numerical software are also applicable in this case study. The curve in Figure 4, obtained from the numerical result, is smooth, whereas the curves from the reference paper [47, 49] may not be smooth due to replotting.

3. Numerical Modelling of the Field Problem

3.1. Input Parameters for the Field-Scale Model. The field-scale clay soil deposit with dimensions 30 m × 30 m × 12 m was considered for the study—the square footing of 3 m × 3 m with a thickness of 0.5 m. The numerical modelling procedure was similar to that of the validation section. After several trials, the modelling dimension was chosen to obtain a complete picture of the soil deformation pattern in both cases. The properties of the clay deposit are the following: cohesive strength, $c_u = 6$ kN/m^2, Young's modulus of clay, $E_c = 1{,}000$ kN/m^2, Poisson's ratio, $\nu = 0.45$, permeability, $k = 8.64 \times 10^{-4}$ m/day [29]. The clay deposit was strengthened by planar geogrid placement below the footing within a sand layer (GRSB) and stone column installation with and without radial geogrid encasement (OSC and GESC).

For the first case, a 0.67 B thick sand layer was placed over the clay deposit, as adopted from Demir et al. [11], where B is the width of the footing. The geogrid is placed at a depth of 0.17 B below the footing [10]. As per the studies by Khing [50], the bearing capacity of the clay deposit with geogrid placed at the sand bed-clay interface was similar to the unreinforced sand bed. The geogrid at the sand bed-clay interface was not provided for the same reason. Also, as per Demir et al. [11], the geogrid depth at 0.67 B below the footing showed slight improvement. Therefore, the geogrid was chosen to be placed closer to the footing.

The width of the geogrid was adopted as 4 B as the bearing capacity increment was assessed to reach up to 95% at this width [1]. Many authors have used a wider dimension of geogrid in past studies [14, 51–54]. The properties of the sand layer are as follows: friction angle, $\varphi = 43°$, unit weight, $\gamma = 21.7$ kN/m^3 [11], Young's modulus, $E = 40{,}000$ kN/m^2 [34].

Four 600 mm diameter end-bearing stone columns were installed in the square arrangement below the footing for the second case. The analyses were conducted for OSC and GESC. 500, 1,000, 2000, 3,000, 4,000, and 5,000 kN/m were chosen as the encasement stiffness. The range of axial stiffness of geogrids was chosen based on practical applications [28]. The properties of the stone column are as follows: friction angle, $\varphi = 48°$, unit weight, $\gamma = 18.4$ kN/m^3, Young's modulus of stone column, $E_s = 10{,}000$ kN/m^2, permeability, $k = 1$ m/day [29]. The modular ratio chosen for the clay + stone column was 10. Based on the study by Barksdale and Bachus [55], for the ratio of Young's modulus of the stone column to that of the clay, $E_s/E_c = 10$, the average SCF was observed to be 3. With that as the assumption, for the modular ratio of 10, the authors considered Young's modulus of the stone column (E_s) as 10,000 kN/m^2 [29].

3.2. Modelling of the Field-Scale Model. The schematic diagrams of the field problem for numerical analysis are shown in Figures 5(a) and 5(b). The remaining modelling part was similar to that explained in the validation portion of this paper.

3.3. Parametric Analyses of the Field Problem. The different cases which were numerically analysed were: (i) footing on the natural clay deposit alone (Figure 6(a)), (ii) footing on the sand layer with a planar geogrid layer (Figure 6(b)), and (iii) footing on the OSC/GESC-reinforced clay deposit (Figure 6(c)). The clay, sand, and stone column properties were kept constant. The axial stiffness of the encasement varied from 500 to 5,000 kN/m, and its effect on vertical stress development and concentration was analysed.

Table 3: Soil and stone column properties for the Validation-2 [47].

Parameters	Desiccated clay layer	Alluvial clay layer	Stone column
Layer thickness (m)	0–1	1–13	—
Material model	M–C	M–C	M–C
Unit weight, γ (kN/m^3)	18.9	18.9	20.6
Undrained shear strength, c_u (kPa)	150	30	—
Angle of internal friction, φ (°)	35	24	47
Young's modulus, E (MPa)	8	3.5	85
Poisson's ratio (ν)	0.45	0.3	0.25

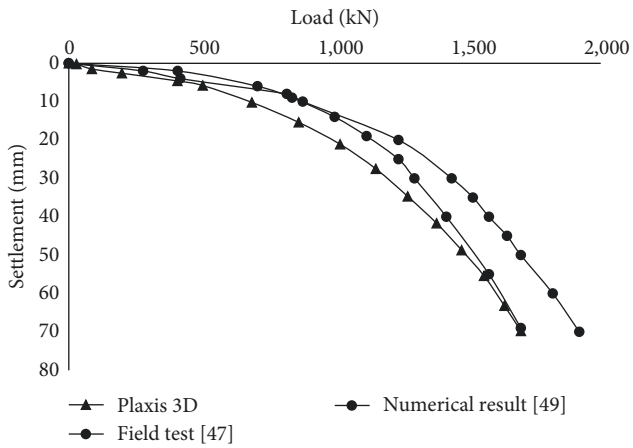

Figure 4: Validation-2— graph comparing field test [47], numerical [49], and PLAXIS 3D (present study) results.

The soil deposit needs to develop a higher level of vertical stress to address the stress distribution. So, the soil has to undergo a larger settlement to develop higher stresses. Numerical analysis carried out by applying load on the soil deposit can sometimes lead to failure, which does not entirely create a stress field in the finite element modelling software. So, the settlement is controlled instead of applying load to develop a stress of higher intensity in the soil deposit. For this reason, the numerical analyses were performed for a prescribed displacement of 0.3 m in the downward direction along the Z axis, equal to 10% of the footing dimension [4], as shown in Figure 6(d).

4. Results and Discussion

The numerical simulation results of the footing with GRSB and OSC/GESC are discussed in this section. The vertical stress development and distribution are expressed at the layers instead of an overall pressure bulb, as the bulb formation is unclear. The footing settlement (S) was presented as a function of the footing dimension (B) [7, 14]. The force developed for the prescribed displacement was used to plot the load vs S/B graph. The following discussions are presented from the vertical stresses developed in the composite ground and the deformation profiles.

4.1. Footing on the GRSB. The analysis results of GRSB are compared with those of the natural clay deposit (unimproved clay) and the unreinforced sand layer, i.e., only the sand layer placed over the clay deposit without any geogrid reinforcement. The vertical stresses observed from the natural clay deposit, unreinforced sand layer, and GRSB are tabulated in Table 4. Vertical stresses are observed at the footing depth, geogrid layer, sand–clay interface, and clay deposit, and their corresponding depths are 0.5, 1, 2, and 2.2 m, respectively. From Table 4, only the depth was considered to interpret the stress values for the natural clay and the unreinforced sand layer, represented by the zero geogrid stiffness.

It should be noted that the transfer of stresses to depths is a function of the sand bed thickness, the first reinforcement depth, length, and number of reinforcements [56]. The discussion here is given for a single reinforcement of length 4 B at a depth of 0.17 B from the base of the footing in a sand bed of 0.67 B thickness. From Table 4 values, it can be observed that there was a gradual but significantly less increase in the vertical stresses with depth for the unimproved clay condition. The vertical stress developed at the bottom of the footing is significantly less for all the cases. In the unreinforced sand layer, vertical stresses increased from 7 kN/m^2 at the footing depth to 518 kN/m^2 at the sand–clay interface and reduced considerably at the clay layer. Similarly, for GRSB, the vertical stress increased approximately from 6 to 270 kN/m^2 at the geogrid depth and reached up to 690 kN/m^2 at the sand–clay interface, and it reduced drastically in the clay deposit to 30 kN/m^2. The unreinforced sand layer exhibits a trend similar to the GRSB, except the vertical stress is lesser than the GRSB's geogrid layer at the 1 m depth and at the sand–clay interface.

The influence of the geogrid layer can be observed for 500 kN/m when compared to the unreinforced sand-bed. However, the axial stiffness from 1,000 to 5,000 kN/m has shown a minor increase in the vertical stresses at the depths under consideration and is much similar to the 500 kN/m, and the same trend is shown in Figure 7 for load vs S/B. From Figure 7, compared to the natural clay, the improvement in the load-bearing capacity of the unreinforced sand-bed layer and the GRSB for all the geogrid stiffnesses is about 87% and 89%, respectively, for the prescribed settlement. Analysing Table 4 and Figure 7 reveals the substantial improvement due to geogrid placement, with no apparent influence from axial stiffness. Hence, a geogrid with an axial stiffness of 500 kN/m should be adequate for the GRSB and can be considered the optimum.

The vertical stress at the geogrid layer increased significantly for the following reasons. As the geogrid carries the

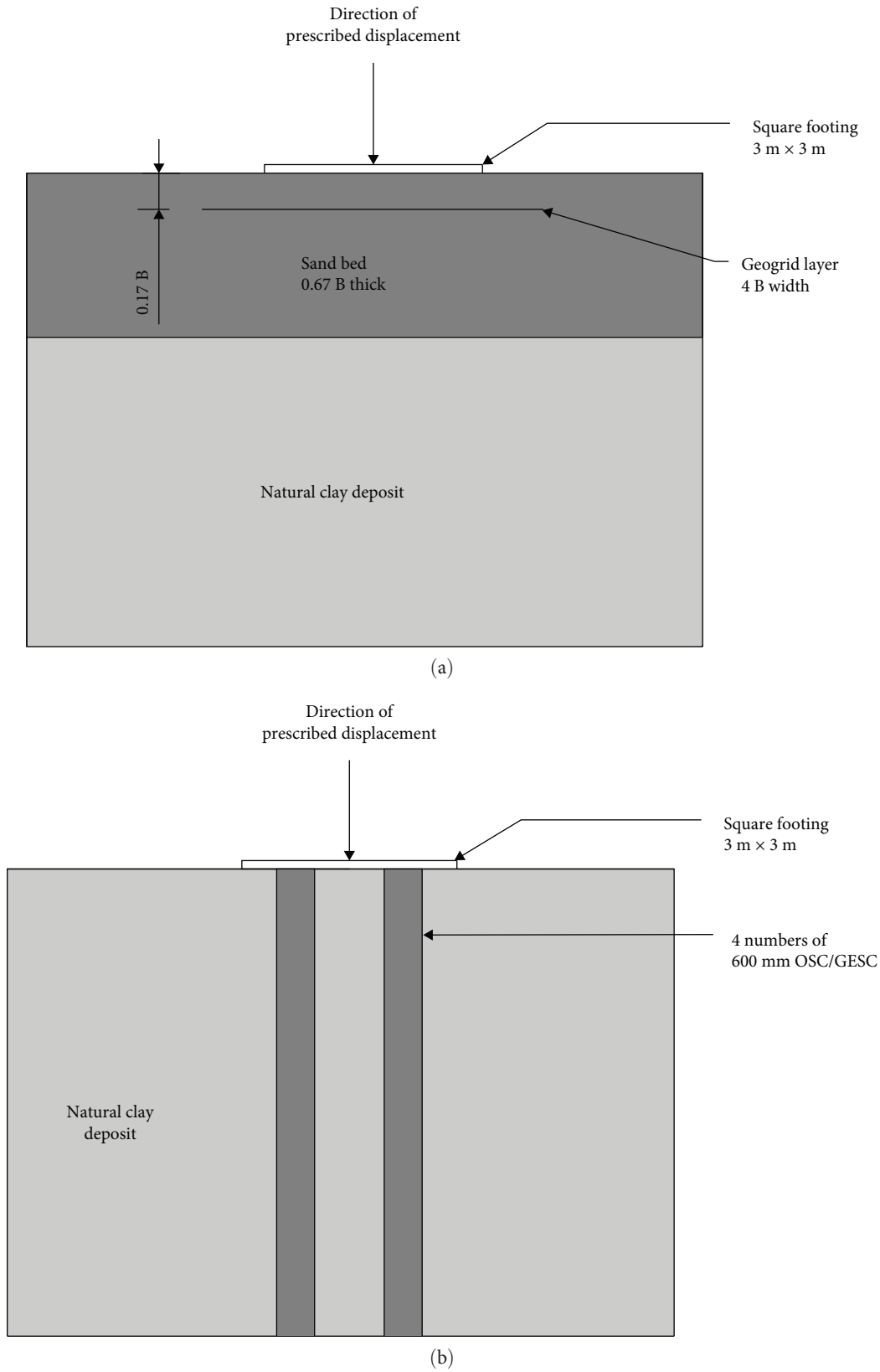

Figure 5: (a) GRSB-installed clay deposit and (b) stone column-installed clay deposit.

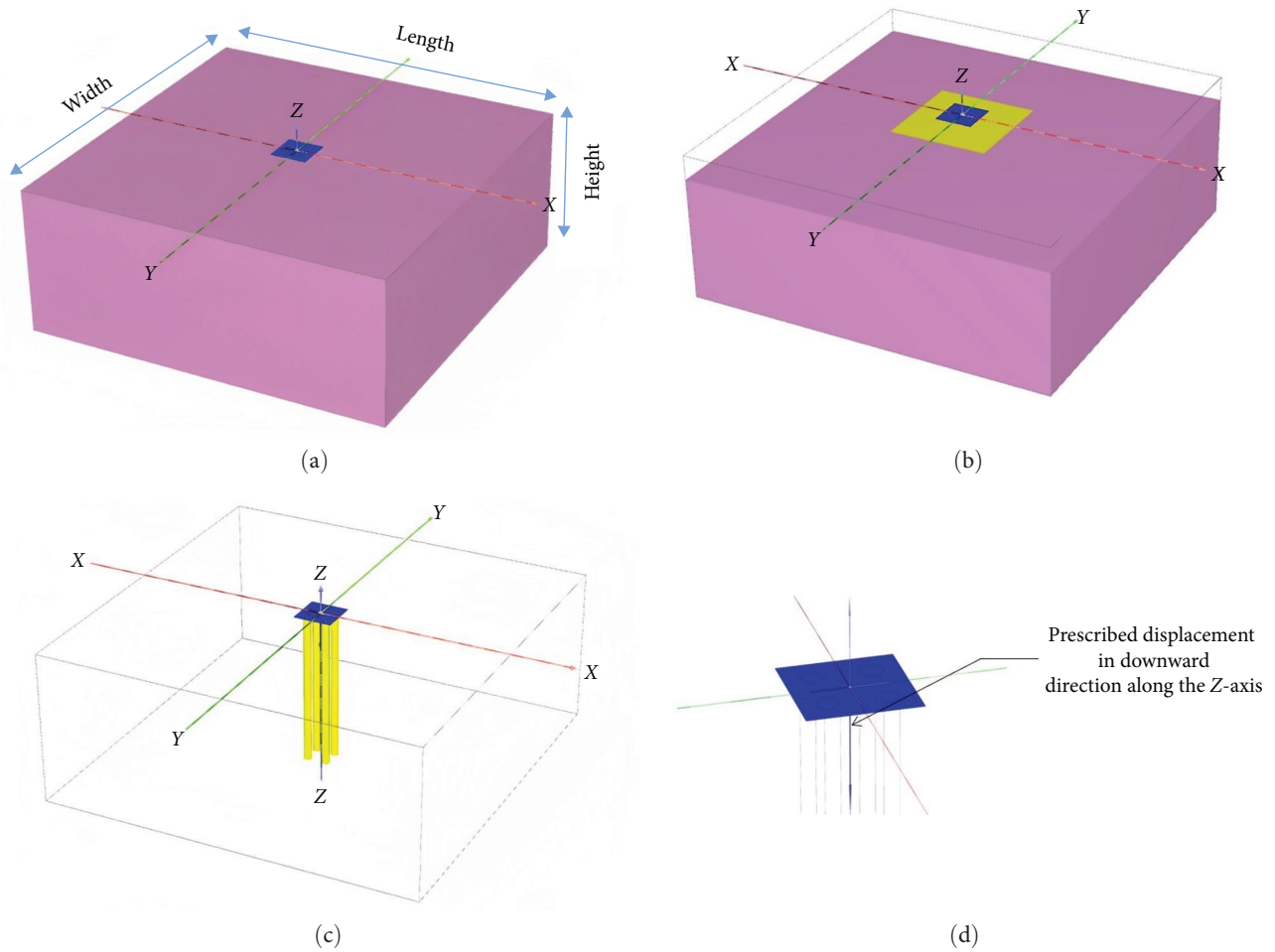

Figure 6: (a) Generalised 3D model—natural clay deposit, (b) generalised 3D model—footing with single layer geogrid, (c) 3D model—Footing with GESC, and (d) footing model showing prescribed displacement.

Table 4: Vertical stresses in the soil at different depths for footing + GRSB.

Geogrid stiffness (kN/m)	Vertical stress (kN/m^2)			
	Footing depth at 0.5 m	Geogrid depth at 1 m	Sand–clay interface at 2 m	Below sand layer at 2.2 m
Natural clay	8.9	14.6	15.0	18.4
0	7.3	128.3	517.7	45.6
500	5.9	269.2	698.6	33.4
1,000	6.1	267.9	694.5	33.3
2,000	6.4	265.3	685.9	33.3
3,000	6.7	262.8	678.1	33.2
4,000	6.9	260.4	670.9	33.2
5,000	7.0	257.9	663.9	33.1

load, the tensile strength gets mobilised by undergoing strain, and vertical stress is developed on this layer. The geogrid's additional length, which is longer than the footing's width, provides anchorage against pull-out resistance [56], thereby developing vertical stress.

The vertical stresses were observed to be the maximum at the sand–clay interface. From this observation, it can be proposed that an additional geogrid at the sand–clay interface could carry higher vertical stresses. The proposed additional layer influences the stress-carrying capacity of the composite foundation if the geogrid layer is placed within the critical depth below the footing. The critical depth of the footing is equal to the footing width [51]. The sand layer is 0.67 B, less than the critical depth. At a depth of 2.2 m, i.e., in clay, the stresses were reduced by about 95% compared to the sand–clay interface at 2 m. A significantly lesser stress developed in

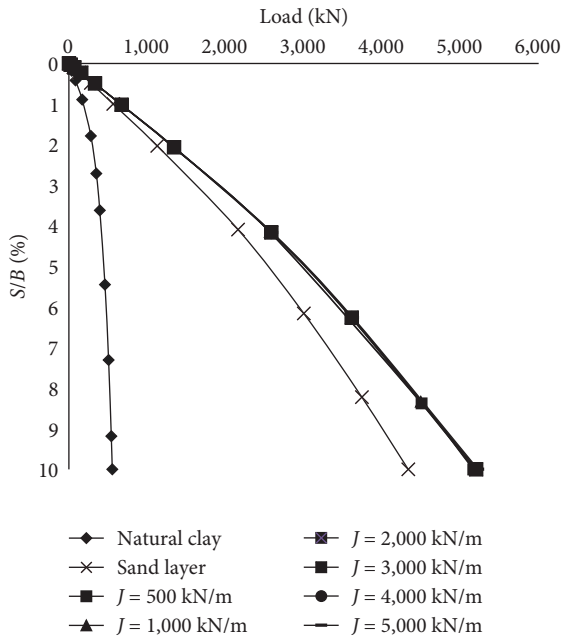

FIGURE 7: Load vs S/B—footing + GRSB.

the clay deposit ensures that only a lesser load is transferred to it, thereby reducing the settlement of the soft clay deposit.

Influence of the geogrid. The geogrid's axial stiffness, which is greater than 1,000 kN/m, reduced the vertical stress by only about 1%. The load-bearing capacity of the GRSB did not appear to be impacted by the axial stiffness, but the geogrid placement itself affected the vertical stress. Past studies also reported that the provision of the geogrid impacts the vertical stress distribution in the soil [13], and it was also documented that the configuration and the layout of the geogrid alone are significant, but not the tensile strength of the geogrid [14]. So, 500 kN/m axial stiffness geogrid would be sufficient for the GRSB.

The vertical stresses that are not transferred to the deeper layers may be due to the geogrid stiffness and length [57]. The reinforcements with a length greater than the footing width can bear the additional development of stresses, thereby preventing the stresses at deeper layers. As mentioned before, the length of the reinforcement has to get the tensile strength mobilised; a part of it must act as the anchorage for providing a pull-out resistance [56]. Therefore, if improving the deeper layers, it can be proposed that reinforcements of optimum width must be placed in several layers within the critical depth of the footing or the shear zone depth below the footing [57]. So, the length and placement depth of the reinforcement play a significant role in the composite foundation.

The vertical stress distribution. The extent of the vertical stresses in the horizontal direction was measured along the geogrid and the sand–clay interface layer. The stresses were observed to be maximum and minimum at 1 and 2.3 B from the centre of the footing at 690 and 20 kN/m^2, respectively. The vertical stresses beyond 2.3 B were lesser than that in the clay deposit. In the vertical direction, the stresses were maximum at the sand–clay interface, as mentioned earlier, which was 0.67 B. The geogrid-reinforced sand layer intercepted the vertical stress distribution with depth, which resulted in a different vertical stress distribution pattern.

4.2. Footing on OSC and GESC. The stone column-installed ground improvement can be expressed through the SCF. SCF is the vertical stress ratio the stone column carries when compared with the surrounding soil below the footing. Generally, the SCF is maximum at the head of the stone column and decreases with increasing length. Moreover, SCF is maximum for rigid footing compared to flexible foundations. With the unit cell concept, the SCF values would be between 2.5 and 5 [23].

As stated earlier, the vertical stresses were measured in the stone columns, and the intervening clay, located at the centre of the four-column arrangement. As the stone column's critical length is twice that of the width of the footing [58], the vertical stresses need to be measured up to 6 m from the column head. But the vertical stresses were prominent only up to 2 m, i.e., 0.67 B, and only those values are presented. SCF values were calculated from the vertical stresses. The vertical stresses were read from the numerical output tables, as shown in Table 5. The vertical stresses from the numerical analysis results in the unimproved clay deposit were 8–20 kN/m^2. However, after the stone column installation, the vertical stress development in clay increased by around 85%. The subsequent paragraphs elaborate on the pattern of the variation in vertical stresses.

Table 5 illustrates the increased vertical stresses in the stone column and clay corresponding to an increment in the encasement axial stiffness at the GL and 1 m below the GL. A similar observation was evident at 2 m below GL in the stone column, whereas the vertical stresses in clay were consistently in the same range, exhibiting a subtle fluctuation with the increase in the encasement axial stiffness. For all the cases of OSC and GESC, there was a noticeable decrement in the vertical stresses with increased depth. Furthermore, there was an apparent prominence in the load-sharing between the stone column and clay, observed from the SCF values reaching 1 at a depth of 2 m. At the GL, the stone columns demonstrated a higher load than the clay, indicated by the SCF values exceeding those at 1 and 2 m depths.

The SCF for OSC and 500 kN/m stiffness geogrid remains the same and exhibits a slight reduction for 1,000 kN/m; beyond this, SCF remains constant. At 1 and 2 m depths, the SCF increases and becomes constant at 500 and 3,000 kN/m, respectively. However, the significance of the SCF calculation lies in ensuring that the stone column minimises the load transfer to the surrounding clay. With that as the criterion, the SCF at the ground surface is evaluated, and the corresponding encasement stiffness of 1,000 kN/m can be taken as the optimum value for improving the clay deposit.

From Figure 8, the load vs S/B curve remains the same for all the geogrid stiffness and OSC, as the minor distinctions were noticeable only in the initial loading region. As the encasement's effect seems negligible in the performance of the load-carrying capacity of the GESC-supported footing, the system was reanalysed for a higher settlement. The

Table 5: Vertical stresses in the soil and stone columns with SCF at different depths for footing + stone column.

Encasement stiffness (kN/m)	Ground level Vertical stress (kN/m^2)			1 m below GL Vertical stress (kN/m^2)			2 m below GL Vertical stress (kN/m^2)		
	Stone column	Clay	SCF	Stone column	Clay	SCF	Stone column	Clay	SCF
0	922.35	808.11	1.14	780.47	734.09	1.06	574.73	589.84	0.97
500	923.26	811.53	1.14	797.6	736.22	1.08	578.14	590.06	0.98
1,000	924.14	814.28	1.13	799.53	737.99	1.08	580.52	590.13	0.98
2,000	925.29	818.39	1.13	802.43	740.52	1.08	584.34	590.06	0.99
3,000	926.39	821.54	1.13	804.69	742.37	1.08	589.87	587.43	1.00
4,000	927.06	823.87	1.13	806.35	743.68	1.08	589.96	589.62	1.00
5,000	929.54	826.88	1.12	808.74	748.58	1.08	592.45	589.72	1.00

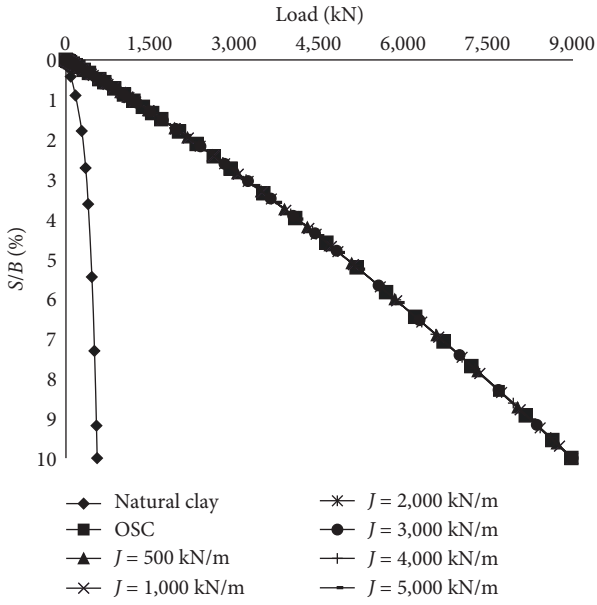

Figure 8: Load vs S/B—footing + stone column.

prescribed settlement (10% B) was increased step by step by 1% of the footing dimension (1% B), and at 17% B, a noticeable difference in the load-carrying capacity of the GESC was observed. The findings revealed a 5% enhancement in the load borne by the GESC with a stiffness of 500 kN/m for the increased settlement. The increase in the load-carrying capacity of GESC can be attributed to the mobilisation of the tensile strength of the encasement when subjected to higher settlement. Therefore, it can be inferred that the encasement can safeguard the stone column, preventing failure, even when subjected to a higher loading. Also, from the practical point of view, the provision of encasement is necessary for confinement to the column material from getting into the soft clay [59].

Additionally, from the analysis results, the vertical stress in the horizontal direction was maximum till the edge of the footing. Beyond the footing edge, the stresses became negligible. So, stress development is prevented beyond the footing edge, which is an advantage of installing stone columns, avoiding interference with the adjacent footings.

Influence of clay, GRSB, and OSC/GESC below the footing. The deformation pattern of the soil below the footing in natural clay, sand, GRSB, and GESC is shown in Figure 9(a)–9(c). The pattern variation interprets the composite ground's different mechanisms against the footing on natural clay. As described earlier, the vertical stress distribution becomes broader in the case of GRSB and is confined within the footing width for the OSC and GESC. The pattern interprets that in GRSB, the vertical stress gets distributed as lesser intensity to deeper depths, preventing the soft soil deposit from the effect of higher stresses. The OSC and GESC confine and bear the load from the footing, preventing the surrounding and underlying soil from the influence of higher stresses.

Comparison of GRSB and OSC/GESC below the footing. In GRSB, the vertical stresses extended up to 2.3 B from the central axis of the footing in the horizontal direction at the location of the sand–clay interface depth of 0.67 B, whereas at the same depth for OSC/GESC, the vertical stresses were confined within the footing width, which indicates no interference of the stresses with the adjacent footings in field conditions. So, stone columns would be a better option in places of limited land width. Also, the OSC and GESC installation improved the clay layer below the depth of 0.67 B to carry higher vertical stresses on par with the stone columns.

For GRSB, the geogrid placement had a significant influence compared with unimproved natural clay and unreinforced sand layers, but the axial stiffness did not influence it. So, the 500 kN/m axial stiffness can be considered optimum for GRSB. In GESC, the encasement confines the stone column material under field conditions and prevents it from spreading in very soft clay soil. The material confinement would make GESC a better option when compared to OSC. Also, the influence of the encasement is noticeable when analysed for a higher settlement. Considering these factors and SCF, the optimum geogrid encasement stiffness is 1,000 kN/m.

The most cost-effective approach among the two techniques depends on variables such as the depth of the weak soil deposit, availability of workforce and construction materials, skilled technicians, equipment, advanced machinery, the extent of the area to be improved, and the project completion period. The cost of the ground improvement technique fluctuates based on these factors. For instance, the GRSB do not require skilled labour or specialised machinery to place the geogrid layer, whereas the stone column installation needs them all. Considering this aspect, the OSC/GESC installation is expensive compared to GRSB. If advanced machinery is

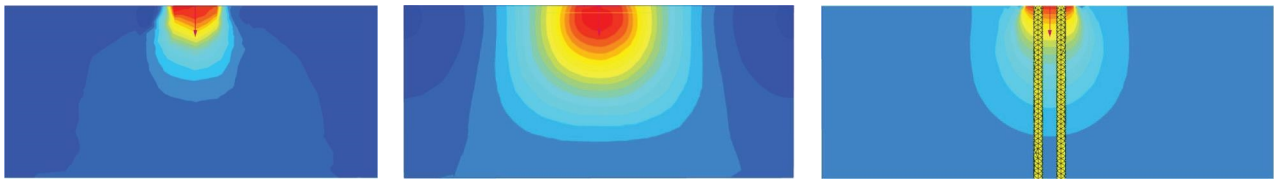

(a) (b) (c)

Figure 9: Deformation pattern of soil below footing in (a) natural clay, (b) GRSB, and (c) GESC.

readily available, a tight project deadline, and there is a large area to improve, choosing OSC/GESC would reduce the overall project cost. As a result, it is essential to acknowledge that this study may not achieve exhaustive coverage of all the factors related to this aspect due to inherent constraints. Consequently, the cost-effectiveness of a particular project can be determined by considering all the factors mentioned above.

5. Conclusions

In this paper, a numerical investigation of the footing supported on (i) a layer of the sand bed with a single-layer geogrid—GRSB and (ii) four numbers of stone columns—OSC and GESC was discussed. The variation in the development of vertical stresses and the ability of the two ground improvement techniques to transfer the vertical stresses can be understood from the results. The conclusions and comparisons for the same are presented below.

5.1. GRSB vs OSC and GESC

(i) The vertical stresses at different depths explain the stress transfer mechanism. This knowledge can allow the practitioners to decide the depth of placement of the reinforcement and also to choose an alternate if one method is not feasible for the site.

(ii) In GRSB, providing a geogrid layer below the footing within the critical depth is mandatory. It is also proposed to provide an additional geogrid layer at the sand–clay interface depth to carry the higher vertical stresses.

(iii) Comparing the extent of the vertical stresses from the central axis of the footing, OSC and GESC would be better options in places of limited land width, preventing the interference of vertical stresses with the adjacent footings.

(iv) The optimum axial stiffness is proposed as 500 kN/m for the GRSB and 1,000 kN/m for the GESC.

The conclusions are for a set of geotechnical conditions deviating from which a new study has to be performed.

Data Availability

Previously reported field data were used for the validation purpose of this study and are available at https://doi.org/10.1016/j.geotexmem.2012.05.007 and https://doi.org/10.1061/(ASCE)1090-0241(2007)133:12(1503). These prior studies [11, 47] are cited at relevant places within the text as a reference.

Conflicts of Interest

The authors declare that there are no conflicts of interest regarding the publication of the paper.

Acknowledgments

The second author acknowledges the fellowship from the University Grants Commission UGC-NFOBC Fellowship (NFO-2018-19-OBC-TAM-73673) for the Ph.D. programme.

References

[1] R. L. Michalowski, "Limit loads on reinforced foundation soils," *Journal of Geotechnical and Geoenvironmental Engineering*, vol. 130, no. 4, pp. 381–390, 2004.

[2] A. M. Krishna and A. Biswas, "Performance of geosynthetic reinforced shallow foundations," *Indian Geotechnical Journal*, vol. 51, no. 3, pp. 583–597, 2021.

[3] N. I. Hasan, A. M. Taib, N. S. Muhammad, M. R. M. Yazid, A. A. Mutalib, and D. Z. A. Hasbollah, "Effectiveness of strip footing with geogrid reinforcement for different types of soils in Mosul, Iraq," *PLOS ONE*, vol. 15, no. 12, Article ID e0243293, 2020.

[4] A. Biswas, A. M. Krishna, and S. K. Dash, "Behavior of geosynthetic reinforced soil foundation systems supported on stiff clay subgrade," *International Journal of Geomechanics*, vol. 16, no. 5, Article ID 04016007, 2016.

[5] J. Boussinesq, "Application of potentials to the study of the balance and motion of elastic solids," in *Mathematics and Analysis*, Gautiher-Villars, Paris, 1885.

[6] M. Abu-Farsakh, Q. Chen, and R. Sharma, "An experimental evaluation of the behavior of footings on geosynthetic-reinforced sand," *Soils and Foundations*, vol. 53, no. 2, pp. 335–348, 2013.

[7] A. Biswas, M. Asfaque Ansari, S. K. Dash, and A. Murali Krishna, "Behavior of geogrid reinforced foundation systems supported on clay subgrades of different strengths," *International Journal of Geosynthetics and Ground Engineering*, vol. 1, no. 3, pp. 1–10, 2015.

[8] M. A. El Sawwaf, "Behavior of strip footing on geogrid-reinforced sand over a soft clay slope," *Geotextiles and Geomembranes*, vol. 25, no. 1, pp. 50–60, 2007.

[9] L. Yadu and R. K. Tripathi, "Effect of the length of geogrid layers in the bearing capacity ratio of geogrid reinforced granular fill-soft subgrade soil system," *Procedia-Social and Behavioral Sciences*, vol. 104, pp. 225–234, 2013.

[10] A. Demir, A. Yildiz, M. Laman, and M. Ornek, "Experimental and numerical analyses of circular footing on geogrid-reinforced

granular fill underlain by soft clay," *Acta Geotechnica*, pp. 711–723, 2014.

[11] A. Demir, M. Laman, A. Yildiz, and M. Ornek, "Large scale field tests on geogrid-reinforced granular fill underlain by clay soil," *Geotextiles and Geomembranes*, vol. 38, pp. 1–15, 2013.

[12] R. Saha and K. D. Subinay, "Bearing capacity of rectangular footings on multi-layer geosynthetic-reinforced granular fill over soft soil," *International Journal of Geomechanics*, no. 9, Article ID 04017069, 2017.

[13] K. Deb, N. Sivakugan, S. Chandra, and P. K. Basudhar, "Numerical analysis of multi-layer geosynthetic-reinforced granular bed over soft fill," *Geotechnical and Geological Engineering*, vol. 25, pp. 639–646, 2007.

[14] G. M. Latha and A. Somwanshi, "Bearing capacity of square footings on geosynthetic reinforced sand," *Geotextiles and Geomembranes*, vol. 27, no. 4, pp. 281–294, 2009.

[15] F. Niculescu-Enache, "The behavior of foundation soil with and without geosynthetic reinforcement," *Constructii*, vol. 14, no. 1, Article ID 61, 2013.

[16] S. Aria, S. K. Shukla, and A. Mohyeddin, "Numerical investigation of wraparound geotextile reinforcement technique for strengthening foundation soil," *International Journal of Geomechanics*, vol. 19, no. 4, Article ID 04019003, 2019.

[17] S. Aria, S. K. Shukla, and A. Mohyeddin, "Behaviour of sandy soil reinforced with geotextile having partially and fully wrapped ends," in *Proceedings of the Institution of Civil Engineers-Ground Improvement*, vol. 174, no. 1, pp. 29–41, 2021.

[18] S. Jaiswal and V. B. Chauhan, "Response of strip footing resting on earth bed reinforced with geotextile with wraparound ends using finite element analysis," *Innovative Infrastructure Solutions*, vol. 6, no. 2, Article ID 121, 2021.

[19] S. Jaiswal, A. Srivastava, and V. B. Chauhan, "Improvement of bearing capacity of shallow foundation resting on wraparound geotextile reinforced soil," *International Foundations Congress & Equipment Expo(IFCEE)*, vol. 65, pp. 2021–2074, 2021.

[20] S. Jaiswal and V. B. Chauhan, "Evaluation of optimal design parameters of the geogrid reinforced foundation with wraparound ends using adaptive FEM," *International Journal of Geosynthetics and Ground Engineering*, vol. 7, no. 4, Article ID 77, 2021.

[21] S. Jaiswal, A. Srivastava, and V. B. Chauhan, "Performance of strip footing on sand bed reinforced with multilayer geotextile with wraparound ends," in *Ground Improvement and Reinforced Soil Structures: Proceedings of Indian Geotechnical Conference 2020*, vol. 2, pp. 721–732, Springer, Singapore, 2022.

[22] S. M. Dasaka, S. Jaiswal, and V. B. Chauhan, "Smart geotechnics for smart societies," in *Proceedings of the 17th Asian Regional Conference on Soil Mechanics and Geotechnical Engineering*, A. Zhussupbekov, A. Sarsembayeva, and V. N. Kaliakin, Eds., CRC Press, London, 2023.

[23] IS: 15284 (part 1), "Indian standard code of practice for design and construction for ground improvement guidelines," New Delhi, 2003.

[24] M. Y. Fattah and Q. G. Majeed, "A study on the behaviour of geogrid encased capped stone columns by the finite element," *GEOMATE Journal*, vol. 3, no. 5, pp. 343–350, 2012.

[25] M. Y. Fattah and Q. G. Majeed, "Finite element analysis of geogrid encased stone columns," *Geotechnical and Geological Engineering*, vol. 30, pp. 713–726, 2012.

[26] M. Y. Fattah, B. S. Zabar, and H. A. Hassan, "Soil arching analysis in embankments on soft clays reinforced by stone columns," *Structural Engineering and Mechanics*, vol. 56, no. 4, pp. 507–534, 2015.

[27] M. Y. Fattah, B. S. Zabar, and H. A. Hassan, "Experimental analysis of embankment on ordinary and encased stone," *International Journal of Geomechanics*, vol. 16, no. 4, Article ID 04015102, 2016.

[28] S. Murugesan and K. Rajagopal, *Geosynthetic-encased stone columns*, vol. 24, no. 6, pp. 349–358, 2006.

[29] P. M. Rajan and P. Krishnamurthy, "Deformation of stone column subjected to earthquake loading by numerical analysis," in *Ground Improvement Techniques: Select Proceedings of 7th ICRAGEE 2020*, pp. 187–200, Springer Singapore, Singapore, 2021.

[30] P. M. Rajan and P. Krishnamurthy, "Termination criteria of bored pile subjected to axial loading," *Indian Geotechnical Journal*, vol. 49, pp. 566–579, 2019.

[31] S. F. Kwa, E. S. Kolosov, and M. Y. Fattah, "Ground improvement using stone column construction encased with geogrid," *Stroitel'stvo Unikal'nyh Zdanij i Sooruzenij*, vol. 3, pp. 49–59, 2018.

[32] V. B. Chauhan, Y. A. Kolekar, and S. M. Dasaka, "Some laboratory and numerical studies on the behaviour of stone columns installed in Mumbai marine clay," in *Soil Testing, Soil Stability and Ground Improvement: Proceedings of the 1st GeoMEast International Congress and Exhibition, Egypt 2017 on Sustainable Civil Infrastructures*, pp. 125–135, Springer International Publishing, 2018.

[33] R. B. J. Brinkgreve, L. M. Zampich, and N. R. Manoj, *PLAXIS CONNECT Edition V20 Manual*, PLAXIS BV, Bentley Systems, Netherlands, 2019.

[34] B. M. Das, *Principles of Geotechnical Engineering*, Cengage Learning, 2021.

[35] K. Terzaghi, R. B. Peck, and G. Mesri, *Soil Mechanics in Engineering Practice*, John Wiley & Sons, 1996.

[36] "Caltrans Geotechnical Manual," 2021, https://dot.ca.gov/programs/engineering-services/manuals/geotechnical-manual.

[37] J. E. Bowles, "Foundation analysis and design," 1988.

[38] R. E. Goodman, *Introduction to Rock Mechanics*, John Wiley & Sons, 1991.

[39] K. W. Cole and M. A. Stroud, "Rock socket piles at coventry point, market way, coventry," *Geotechnique*, vol. 26, no. 1, pp. 47–62, 1976.

[40] A. Fawaz, F. Hagechehade, and E. Farah, "A study of the pressuremeter modulus and its comparison to the elastic modulus of soil," *Study of Civil Engineering and Architecture (SCEA)*, vol. 3, pp. 7–15, 2014.

[41] M. R. Lindeburg, *Civil Engineering Reference Manual for the PE Exam*, Professional Publications, 1999.

[42] BS 8006-1: 2010, *Code of Practice for Strengthened/Reinforced Soils and Other Fills. Design of Embankments with Reinforced Soil Foundations on Poor Ground*, British Standards Institution (BSI), 2010.

[43] R. A. Jewel, "Soil reinforcement with geotextile," *CIRIA, Special Publication*, vol. 123, 1996.

[44] M. Shinoda and R. J. Bathurst, *Strain measurement of geogrids using a video-extensometer technique. Geotechnical testing*, vol. 27, no. 5, pp. 456–463, 2004.

[45] M. H. Wayne, J. Han, and K. Akins, *The Design of Geosynthetic Reinforced Foundation*, ASCE's Annual Convention & Exposition, Boston, Massachusetts, 1998.

[46] J. L. M. Clemente, T. Liao, and T. Nixon, "Geogrid-reinforced soil mat for temporary support of heavy equipment," 2008.

[47] D. J. White, H. T. V. Pham, and K. K. Hoevelkamp, "Support mechanisms of rammed aggregate piers. I: experimental

results," *Journal of Geotechnical and Geoenvironmental Engineering*, vol. 133, no. 12, pp. 1503–1511, 2007.
[48] IS 456: 2000 (R2016), "Plain and reinforced concrete. Code of practice (4th revision)," Standard, Indian, and IS, 2000.
[49] H. T. V. Pham and D. J. White, "Support mechanisms of rammed aggregate piers. II: numerical analyses," *Journal of Geotechnical and Geoenvironmental*, vol. 133, no. 12, pp. 1512–1521, 2007.
[50] K. H. Khing, B. M. Das, V. K. Puri, S. C. Yen, and E. E. Cook, "Strip foundation on sand underlain by soft clay with geogrid reinforcement," in *The Third International Offshore and Polar Engineering Conference*, OnePetro, 1993.
[51] M. R. DeMerchant, A. J. Valsangkar, and A. B. Schriver, "Plate load tests on geogrid-reinforced expanded shale lightweight aggregate," *Geotextiles and Geomembranes*, vol. 20, no. 3, pp. 173–190, 2002.
[52] M. T. Omar, B. M. Das, V. K. Puri, and S. C. Yen, "Ultimate bearing capacity of shallow foundations on the sand with geogrid reinforcement," *Canadian Geotechnical Journal*, vol. 30, no. 3, pp. 545–549, 1993.
[53] A. Akbar, J. A. Bhat, and B. A. Mir, "Plate load tests for investigation of the load–settlement behaviour of shallow foundation on bitumen-coated geogrid reinforced soil bed," *Innovative Infrastructure Solutions*, vol. 6, no. 2, Article ID 80, 2021.
[54] H. A. Alawaji, "Settlement and bearing capacity of geogrid-reinforced sand over collapsible soil," *Geotextiles and Geomembranes*, vol. 19, no. 2, pp. 75–88, 2001.
[55] R. D. Barksdale and R. C. Bachus, *Design and Construction of Stone Columns*, US Department of Transportation, Federal Highway Administration, 1983.
[56] R. P. Rethaliya and A. K. Verma, "Strip footing on sand overlying soft clay with geotextile interface," *Indian Geotechnical Journal*, vol. 39, no. 3, pp. 271–287, 2009.
[57] E. Cicek, E. Guler, and T. Yetimoglu, "Stress distribution below a continuous footing on geotextile-reinforced soil," *International Journal of Geomechanics*, vol. 18, no. 3, Article ID 06018005, 2018.
[58] M. Miranda, J. Fernández-Ruiz, and J. Castro, "Critical length of encased stone columns," *Geotextiles and Geomembranes*, vol. 49, no. 5, pp. 1312–1323, 2021.
[59] H.-G. Kempfert and B. Gebreselassie, *Excavations and Foundations in Soft Soils*, Springer Science & Business Media, 2006.